Numerical study of the applicability of the η-factor method to J-resistance curve determination of steam generator tubes using non-standard specimens

CrossMark

Marcos A. Bergant [a,*], Alejandro A. Yawny [b], Juan E. Perez Ipiña [c]

[a] *Proyecto CAREM, Centro Atómico Bariloche (CNEA), Av. Bustillo 9500, San Carlos de Bariloche 8400, Argentina*
[b] *División Física de Metales, Centro Atómico Bariloche (CNEA)/CONICET, Av. Bustillo 9500, San Carlos de Bariloche 8400, Argentina*
[c] *Grupo Mecánica de Fractura, Universidad Nacional del Comahue/CONICET, Buenos Aires 1400, Neuquén 8300, Argentina*

A R T I C L E   I N F O

A B S T R A C T

The suitability of the η-factor method for the determination of J-resistance curves of thin walled steam generator tubes was evaluated using elastoplastic finite element analysis. Different candidate non-standard specimens' geometries were considered. It was shown how high constraint conditions associated with deep cracks geometries and prevailing bending loads favor the η-factor validity while low constraint configurations resulted in a η-factors exhibiting a higher dependence on the applied load. It was also verified that η-factors based on the crack mouth opening displacement (*CMOD*) showed much less dependency on the loading level than η-factors derived from load line displacement (*LLD*).

© 2015 Elsevier Ltd. All rights reserved.

1. Introduction

The steam generators are heat exchangers consisting in several thousands of tubes arranged inside a pressure vessel. The tubes separate the primary and secondary cooling systems of a nuclear power reactor, isolating the primary coolant and thus avoiding the leak of radioactive elements to the secondary circuit. Due to the negative impact related to their failures, the structural integrity assessment of these components has started receiving special attention.

In order to minimize and anticipate tube failures, much effort has been invested in developing appropriate methodologies for assessing the structural integrity of tubes with defects such as cracks. Since the steam generator tubes (SGTs) materials exhibit a ductile behavior characteristic of austenitic microstructures, elastic–plastic fracture mechanics (EPFM) is one of the methodologies that has recently started to be used for this purpose [1–4]. Its application to structural integrity analysis requires the experimental characterization of the material fracture toughness in terms of, for example, J-resistance curves.

However, the high fracture toughness and the reduced characteristic dimensions of SGTs (diameters between 12 and 20 mm and wall thicknesses between 1 and 2 mm) results in the impossibility of obtaining standard specimens for J-resistance curves determination which assure plane strain conditions. It is then understandable why the number of

Nomenclature

a	crack length or half-crack length
B	specimen thickness
$CMOD$	crack mouth opening displacement
$CMOD_{pl}$	plastic component of $CMOD$
C(T)	compact tension specimen
E	Young's elastic modulus
EPFM	elastic–plastic fracture mechanics
J	J-integral
J_{el}	elastic component of the total J-integral
J_{pl}	plastic component of the total J-integral
K_I	mode I linear elastic stress intensity factor
LLD	load line displacement
LLD_{pl}	plastic component of LLD
M(T)	middle tension specimen
P	load
s	slenderness ratio
SE(B)	single-edge-notched bending specimen
SGT	steam generator tube
TWC	through-wall crack
U_{pl}	plastic work
W	specimen width
γ	crack growth correction factor
η	calibration factor
η_{CMOD}	η-factor based on $CMOD$
η_{LLD}	η-factor based on LLD
v	Poisson's ratio

references in the open literature dealing with the experimental determination of the fracture toughness of SGTs in terms of EPFM parameters is rather scarce [2,4,5]. Among those few authors, Huh et al. [2] performed J-resistance tests in Inconel 600 SGTs, using specimens with circumferential through-wall cracks (TWCs) subjected to tensile load. More recently, Sanyal and Samal [5] presented J-resistance curves for longitudinal TWCs in Incoloy 800 SGTs using the pin-loaded tension test, while Bergant et al. [4] reported J-resistance curves for Incoloy 800 SGTs with circumferential cracks under tensile loads.

The η-factor method is the usual approach for estimating the value of J-integral from the load–displacement record obtained in a fracture test. By definition, for a given specimen geometry and load type, η is constant and independent of the load level. Strictly speaking, the possibility of defining a parameter η and its validity must be verified for each type of specimen geometry and loading mode. In a previous work [4], a non-standard experimental technique for J-resistance curves estimation was presented. Specimens were fabricated from straight parts of steam generator tubes, with one or either two circumferential TWCs, and were tested under pure tension. J-integral values were estimated through the η-factor method. It has been found that during the tests, the specimens developed generalized plastic deformation and geometric distortion. Paris et al. [6] noticed that widespread plasticity during loading could invalidate the η-factor existence. In view of that, a numerical study was performed to verify the validity of its application. Former results presented in the previous work showed that the use of the η-factor is not strictly valid for tests involving relatively shallow cracked specimens [4]. In those cases, a dependence of the η-factor with the level of strain (or load and J-integral) was observed. Due to that, an averaging approach was adopted to define the η-factors and J-resistance curves were then estimated for circumferential TWCs in Incoloy 800 SGTs at room temperature.

The possibility of overcoming the just mentioned drawbacks constitutes the aim of the present study. This paper presents an in depth numerical study of the applicability of the η-factor method to different non-standard specimens, being the final objective the recommendation of the most appropriate geometry for a reliable assessment of J-resistance curves of SGTs. Both circumferential and longitudinal cracks have been considered because both orientations were found during in-service inspections of SGTs [7], justifying the interest in the study of both types of cracks. On the other hand, considering that the typical failure mode of cracked SGTs is bursting due to membrane stresses originated in the pressure difference across the tube wall, specimens modeling this actual stress condition are also proposed. Therefore, specimens subjected to prevailing bending and tensile loadings were studied, resulting respectively in both high and low constraint testing conditions.

2. Theoretical background

2.1. J-integral estimation for a stationary crack through the η-factor

The ductile fracture process occurs by initiation and stable growth of a crack. This process is usually conveniently described by a rising curve, i.e., the *J*-resistance curve, which represents the toughness as a function of ductile crack growth. During an elastoplastic fracture test, the specimen is monotonically loaded to produce the stable crack growth. The load *P* and the load line displacement *LLD* are recorded, while the stable crack growth is monitored.

The fracture toughness in terms of the *J*-integral parameter is usually expressed as a sum of elastic and plastic components [8]:

$$J = J_{el} + J_{pl} = \frac{K_I^2}{E/(1 - v^2)} + J_{pl} \tag{1}$$

where K_I is the (Mode I) linear elastic stress intensity factor, *E* is the Young's elastic modulus and *v* is the Poisson's ratio.

Rice et al. [8] interpreted the plastic component, J_{pl}, as the rate of change of potential energy per unit cracked area. From this energy based definition, Sumpter and Turner [9] proposed that J_{pl} can be related to the plastic area under the *P* vs. *LLD* curve. For a particular (*P*; *LLD*) point on that curve, the following relation was proposed:

$$J_{pl} = -\frac{1}{B}\frac{dU_{pl}}{da} = \eta \frac{U_{pl}}{Bb} \tag{2}$$

Here U_{pl} is the plastic work calculated from the area under the *P* vs. *LLD* record until the point (*P*; *LLD*), the derivative of second term represents the variation of U_{pl} with an increment in the crack length *a* at the point (*P*; *LLD*), *B* is the specimen net section thickness, *b* the un-cracked ligament length and *η* is a calibration factor. The *η*-factor is a non-dimensional parameter which is assumed to depend on the flawed geometry and loading type (e.g., bending or tension) but independent of the loading magnitude *P*.

The main advantage of using the *η*-factor for *J*-integral evaluations is its simplicity along with the use of a single specimen. This is in contrast with the multispecimen technique inspired on the energy based definition of the *J*-integral [10]. On the other hand, J_{pl} evaluations based on the *η*-factor requires knowing its appropriate values for the specific geometry and loading mode. The possibility of estimating an appropriate *η*-factor for the non-standard specimen geometries proposed in the present work will be addressed in the next section.

It is important to remark here that the *LLD* involved in the evaluation of the different terms in Eq. (2) includes only the contribution due to the presence of the crack [10]. This means that the displacement associated with the defect-free specimen has to be subtracted from the total displacement of the cracked specimen to evaluate the plastic area U_{pl}. In most of the cases the displacement of the uncracked specimen is negligible and the subtraction is unnecessary. This is particularly true in the case of standardized specimens with deep cracks.

2.1.1. The existence and uniqueness of the η-factor

Paris et al. [6] and Ernst et al. [10] have shown that it is not always possible to express the *J*-integral through the *η*-factor in the way expressed by Eq. (2), i.e., exclusively depending on the particular specimen geometry and loading type but independent of load or level of deformation. These authors explored the necessary and sufficient conditions for the existence of the *η*-factor. They showed that the *η*-factor will exist if and only if the dependence of the load *P* with the geometry of the specimen expressed as a function of the ratio *a*/*W* characterizing the crack depth and the plastic displacement LLD_{pl} can be expressed as separate terms in the form:

$$P = h(a/W) \cdot g(LLD_{pl}) \tag{3}$$

where *h*(*a*/*W*) is a function of *a* solely and does not depend on material properties. This means that plots of *P* vs. LLD_{pl}, for different relations *a*/*W*, must show a scaling relationship if the separation of variables exists, at least for certain ranges of *a*/*W* and LLD_{pl}. The function $g(LLD_{pl})$ is related with the deformation behavior of the specimen, depending only on the material properties. The relationship in Eq. (3), which was assumed in the derivation of the *η*-factor, must be fulfilled in order to ensure the existence of the *η*-factor.

On the other hand, Paris et al. [6] pointed out that if the nature and location of plasticity present radical changes during loading, then the *η*-factor may not exist because the widespread plasticity limits the separation of variables condition for the *η*-factor existence. However, Turner [11] proposed a method to overcome this effect, estimating *η*-factors in an approximate way by considering only the part of the potential energy related to the crack growth (subtracting the energy associated with the widespread plasticity from the total one). In practice, it is possible to measure the crack mouth opening displacement *CMOD*, calculating the area under the *P* vs. *CMOD* (which is mainly associated with the crack growth process), and estimating the *J*-integral through *η*-factors derived for *CMOD*. Also, others researches [12–14] showed that the *η*-factors derived for *CMOD* are less sensitive to the loading or deformation levels and the material properties (i.e. strain hardening and yield stress) than the *η*-factors derived for *LLD*, specially for shallow cracks. Other practical advantages of using the *CMOD* are the higher accuracy of the measurement (the measurement of the *LLD* is less accurate and more difficult because of

transducer mounting difficulties, specimen load point indentations and load train deflections) and the absence of a component for the specimen without crack to subtract to the specimens P vs. $CMOD$ record.

Generally speaking, the η-factor exists when the plastic strain related to the fracture process is confined to the remaining ligament. This condition is verified in practice by using standard specimens with deep cracks. In these cases, the standards provide the value of the η-factor for a given type of specimen and crack length. In the case of non-standard specimens, some proposals for the η-factor values can be found in literature only for common geometries and loading conditions [15,16]. In general, these η-factors are obtained using methods assuming that the separation of variables is valid. However, this condition is not always fulfilled, particularly for low constraint tests (i.e., for relatively shallow cracks or tensile loading) and high strain hardening materials. Therefore it is relevant to study the applicability of the η-factor method for the different non-standard specimen geometries considered in the present work as candidate probes for assessing the J-resistance curves of SGTs.

2.2. J-integral estimation for a growing crack using LLD and CMOD data

All expressions for estimating J_{pl} discussed so far were derived for stationary (non-growing) cracks, in which the non-linearity between the P vs. LLD behavior is due to plastic deformation only. When there is stable growth during the test, a new contribution to the non-linearity appears. The higher the crack growth, the larger the error in the estimation of the J_{pl} when using expressions for non-growing cracks.

Thus, a general equation to evaluate J_{pl} from experimental data was proposed by Ernst et al. [10]. It considers a crack growth correction through the introduction of a γ-factor. The resultant expression is:

$$J_{pl} = \frac{\eta}{bB} \int_0^{LLD_{pl}} P\, dLLD_{pl} - \frac{\gamma}{b} \int_{a_0}^{a} J_{pl}\, da \qquad (4)$$

where a_0 is the initial crack length, and

$$\int_0^{LLD_{pl}} P\, dLLD_{pl} = U_{pl} \qquad (5)$$

The γ-factor is related to the η-factor through [10]:

$$\gamma = \eta - 1 + \frac{b}{W}\frac{d\eta}{d(b/W)} \qquad (6)$$

Therefore, if the η-factor as a function of the crack length a is known, then the correction γ-factor can be derived straightforwardly. It should be noted that the Eq. (6) is strictly valid only when the J-integral estimation is performed from LLD data (i.e., for η_{LLD}-factors). In the particular case where the $CMOD$ is proportional to the LLD data, Eq. (6) may also be used to derive γ-factors for $CMOD$ data [17].

3. Fracture specimens for steam generator tubes

Typically, SGTs have reduced dimensions that demanded the design of non-standardized fracture specimens, presented in Figs. 1 and 2. Circumferential and longitudinal TWCs were considered, since the nuclear industry experience has shown that both types of defects have been found [7]. Also, it is worth mentioning that there are no researches dealing with the fracture properties for circumferential and longitudinal cracks in the same SGT, i.e., the anisotropy on fracture properties has not been studied in SGTs.

The classical approach in fracture mechanics is to determine lower bound material properties through high constraint tests. Therefore, conservative assessments can be performed since the conditions present in the component are less severe. However, if this approach is excessively conservative, more accurate assessments can be performed using information obtained from testing "structure-like" test pieces, i.e., using specimens able to model the actual stress conditions in the component under consideration. Therefore, with this simple approach the specimens realistically model the component related to its thickness and loading mode without considering validity requirements [18].

In our particular case, several researches revealed that tube bursting is the most important failure mode for SGT integrity for normal and accident loading conditions [7]. This condition corresponds to a gross structural failure of the tube wall in which an unstable opening displacement (e.g., opening area increased in response to constant pressure) accompanied by ductile plastic tearing of the tube material occurs. This failure mode is mainly controlled by membrane stresses due to the pressure difference across the tube wall, which is considered a relatively low constraint loading condition.

Therefore, in order to cover both approaches, high and low constraint specimens are proposed in this work. The former condition is reached in specimens subjected to bending loading, while the low constraint state is obtained under tensile states.

Figs. 1 and 2 present all the non-standardized fracture specimens considered. Typical dimensions of the testing configurations are presented in the figures, coinciding with the geometries modeled with the finite elements technique. Fig. 1 shows the specimens with circumferential cracks, which are obtained from straight sections of tubes with one and two opposite
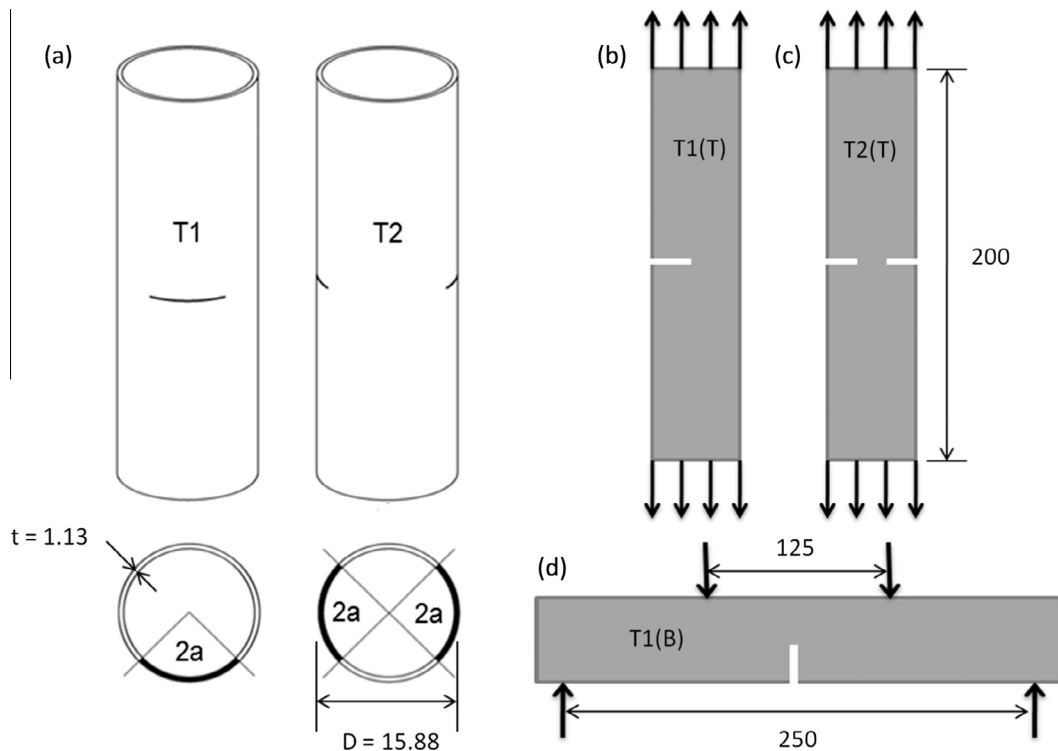
Fig. 1. Specimens with circumferential TWCs: (a) Straight sections of SGTs with one and two opposite TWCs; (b) T1(T), (c) T2(T), (d) T1(B) specimens (dimensions in mm).

circumferential TWCs, Fig. 1(a). The first option, i.e., the tubes with one circumferential TWC, can be loaded in tension or bending resulting in two test configurations, Fig. 1(b) and (d). These specimens were denoted as T1(T) and T1(B), where T1 corresponds to a tubular specimen with one TWC and the letter in brackets (T or B) indicates a tensile or bending loading, respectively. The specimens made with tubes with two opposite TWCs were considered for testing under tension, and were called as T2(T), where T2 refers to a tubular specimen with two cracks, Fig. 1(c). In both tensile test configurations, the ends of the specimens were considered clamped. In the hypothetical case a free tube like the T1(T) specimen were subjected to pure axial tensile stress, its ends will tend to rotate due to the unsymmetrical circumferential crack. However, in a real experiment, the constraint imposed by the clamped ends avoids this rotation introducing a bending moment, which will exert a closing action on the crack faces [4]. To overcome this effect, the T2(T) specimen was designed with two symmetric opposing cracks leading to a more symmetrical condition for axial loading.

Fig. 2 presents the specimens designed with longitudinal cracks. In this case, the manufacture of these specimens requires more effort given the small sizes of the SGTs. A special fabrication procedure outlined in Fig. 2(a) is proposed with the aim of preserving a circumference arc of the tube without plastic deformation, i.e., maintaining the original thermomechanical state of the SGTs. In order to get symmetric loading conditions, specimens were fabricated by welding two half-specimens obtained with the mentioned procedure. The longitudinal cracks are later introduced in this region of unaltered material. Fig. 2(b) presents the specimen called SE(B) "O" by analogy with a single-edge-notched bend specimen (SE(B)), while the "O" refers to the figure generated due to the bonding of the two half-specimens. Fig. 2(c) and (d) exhibit two compact-like specimens, hence identified as C(T) "X" and C(T) "O" following the previous criteria. In the C(T) "X" configuration, the outside diameters of the original tubes were put in contact in order to prevent the buckling of the remnant ligament in compression. Finally, Fig. 2(e) presents the middle tension or M(T) "O" specimen.

The constraint levels in each test configuration presented previously depend on specimen geometry and loading conditions. As the specimen thickness is directly related to the tube wall thickness, the specimen geometric constraint is mainly controlled by the "in plane" dimensions, i.e., the relation a/W. However, it is also known that the geometry of the remaining ligament can also affect the constraint conditions and, therefore, the fracture toughness [18]. It has been shown that with increasing slenderness, defined as the ratio $s = b/B$, the crack resistance increases to a saturation at $s = 3–4$, while the a/B ratio should exceed a value close to 4 [19,20]. As the specimen thickness B (or tube wall thickness) is usually small, the above relations are easily fulfilled with the dimensions indicated in the Figs. 1 and 2.

On the other hand, the constraint condition is also dependent on the loading mode. It is well known that bending components promote a decrease on crack resistance, while tensile modes lead to higher resistance curves [18].
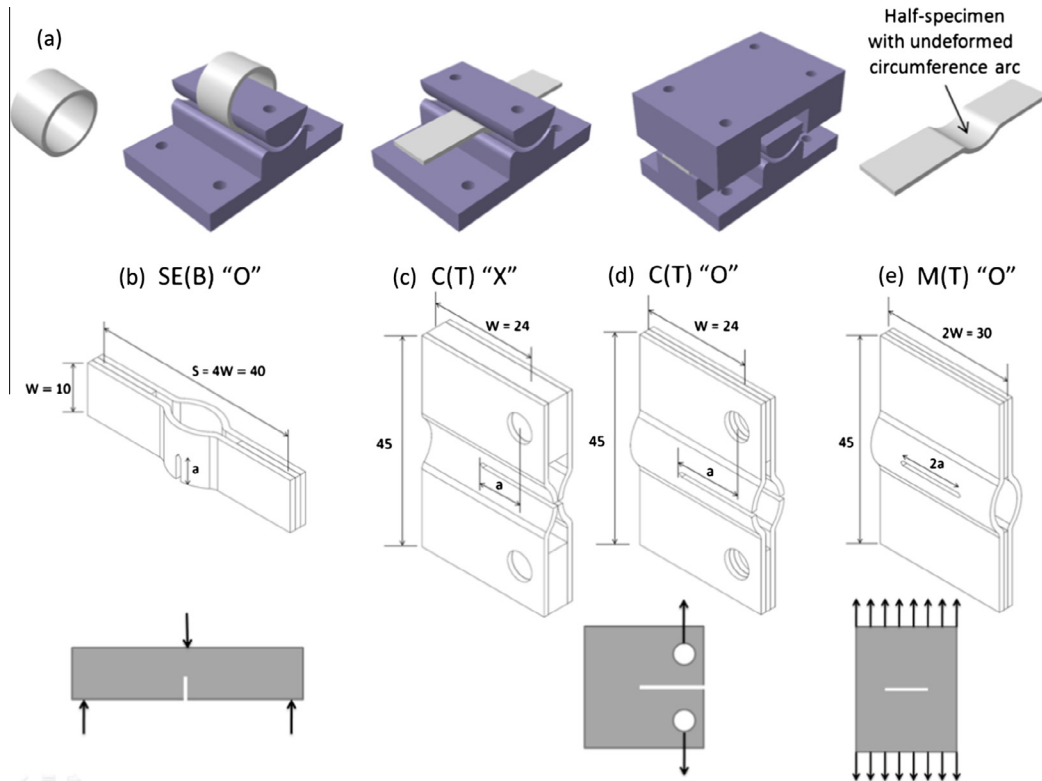
Fig. 2. Specimens with longitudinal TWCs: (a) Extraction process of half-specimens; (b) SE(B) "O", (c) C(T) "X", (d) C(T) "O" and (e) M(T) "O" specimens (dimensions in mm).
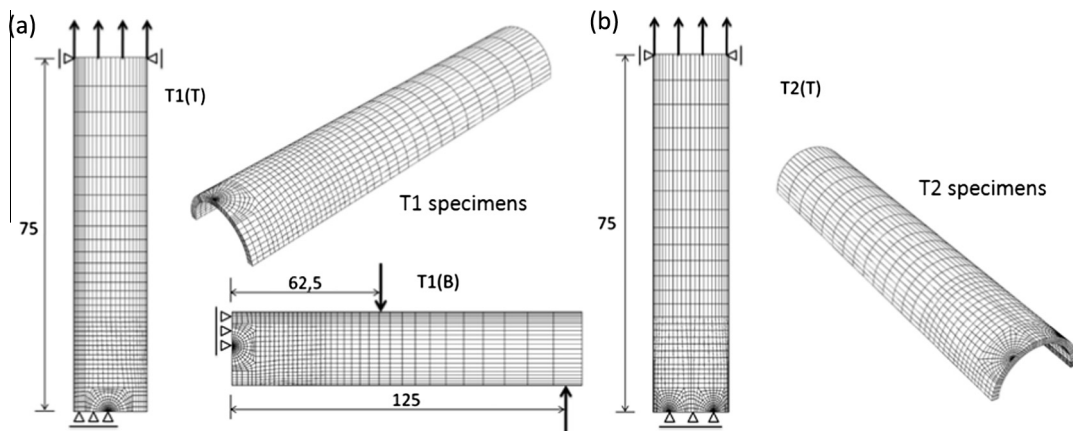

Fig. 3. Finite element meshes for specimens with circumferential TWCs: (a) T1 specimens and (b) T2 specimens (dimensions in mm).

Taking in mind the previous concept, it is possible to classify the presented specimens for low or high constraint testing conditions. The tensile specimens (T1(T) and T2(T) for circumferential cracks and M(T) "O" for longitudinal cracks) promote low constraint levels, whereas the bending mode specimens (T1(B) for circumferential cracks and SE(B) "O", C(T) "O" and C(T) "X" for longitudinal cracks) represent high constraint conditions.

4. The η-factor estimation from finite element analyses

4.1. Numerical procedure

Finite element analyses were conducted to estimate the η-factor values for different test configurations, and to verify the applicability of the η-factor method for the *J*-integral estimation. The finite element code Abaqus 6.12-1 was used. Numerical

3D models for the different specimens with stationary cracks were developed, varying the relations a/W between 0.4 and 0.7. Using symmetry considerations, one-quarter of the specimens were modeled applying proper boundary conditions. The specimens were loaded until the plastic collapse. The actual material stress vs. strain curve measured by means of laboratory tensile tests of Incoloy 800 SGTs was used for the numerical simulations [4]. A focused mesh was designed to provide detailed resolution of the near-tip stress–strain fields, using 3D 20-node quadratic brick elements with reduced integration and a finite strain analysis. The tube thickness was modeled using five elements. Figs. 3 and 4 present the mesh details for the one-quarter specimens with circumferential and longitudinal TWCs, respectively. Boundary conditions and geometric dimensions are added in the figures.

From the finite element analyses, the load P, the displacements LLD and $CMOD$, the rotations at loading points and the J-integral values were obtained. The elastic and the non-crack system displacement or rotations components were subtracted from the total ones. In order to obtain the plastic part of J, the elastic component was subtracted from the total J. The latter was computed using the actual stress vs. strain curve of the material, while the elastic part of J was estimated using the same numerical model but with an elastic behavior. In both cases, J-integral values were calculated through the domain integral method implemented in Abaqus 6.12-1 [21,22].

The J-integral value for each load level was obtained by averaging the individual values of the five elements through the thickness.

The η-factors were calculated solving Eq. (2), from the J-integral values and plastic area under the P vs. displacement numerical results. For all cases, η-factor values were derived from the plastic component of the LLD_{pl}, and from the plastic component of the $CMOD_{pl}$. Then, the plastic component of the J-integral can be expressed as:

$$J_{pl} = \frac{\eta_{LLD}}{Bb} \int_0^{LLD_{pl}} P\, dLLD_{pl} \tag{7}$$

or equivalently:

$$J_{pl} = \frac{\eta_{CMOD}}{Bb} \int_0^{CMOD_{pl}} P\, dCMOD_{pl} \tag{8}$$

where η_{LLD} is an LLD-based geometry factor, and η_{CMOD} is the $CMOD$-based geometry factor.
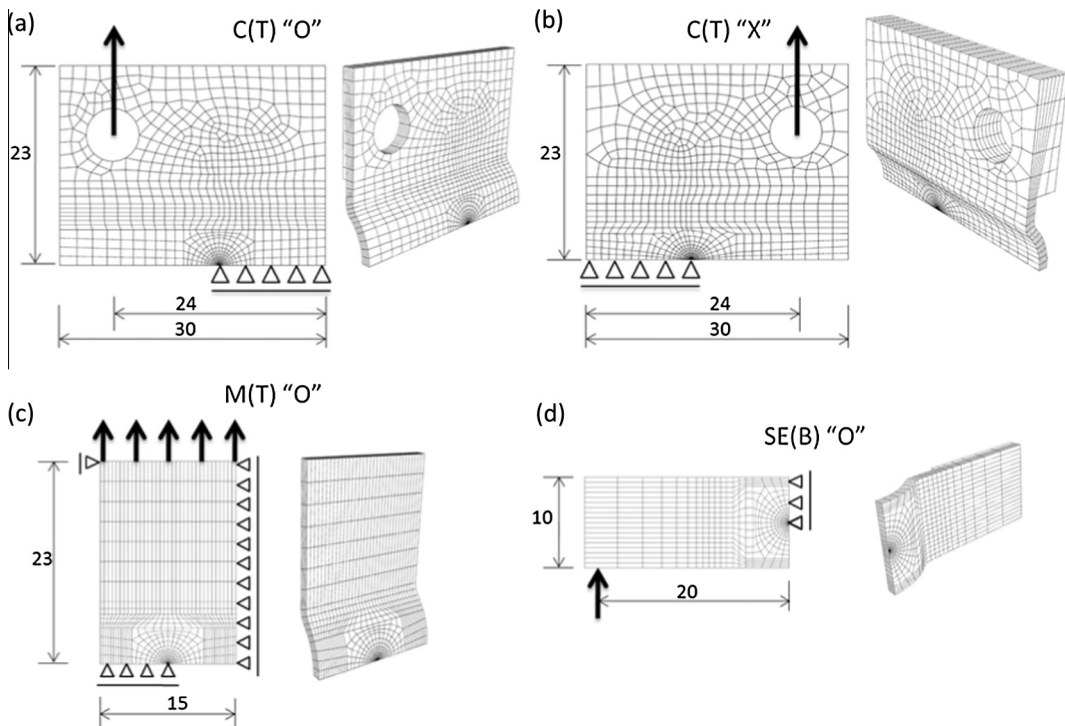

Fig. 4. Finite element meshes for specimens with longitudinal TWCs: (a) C(T) "O", (b) C(T) "X", (c) M(T) "O" and (d) SE(B) "O" specimens (dimensions in mm).
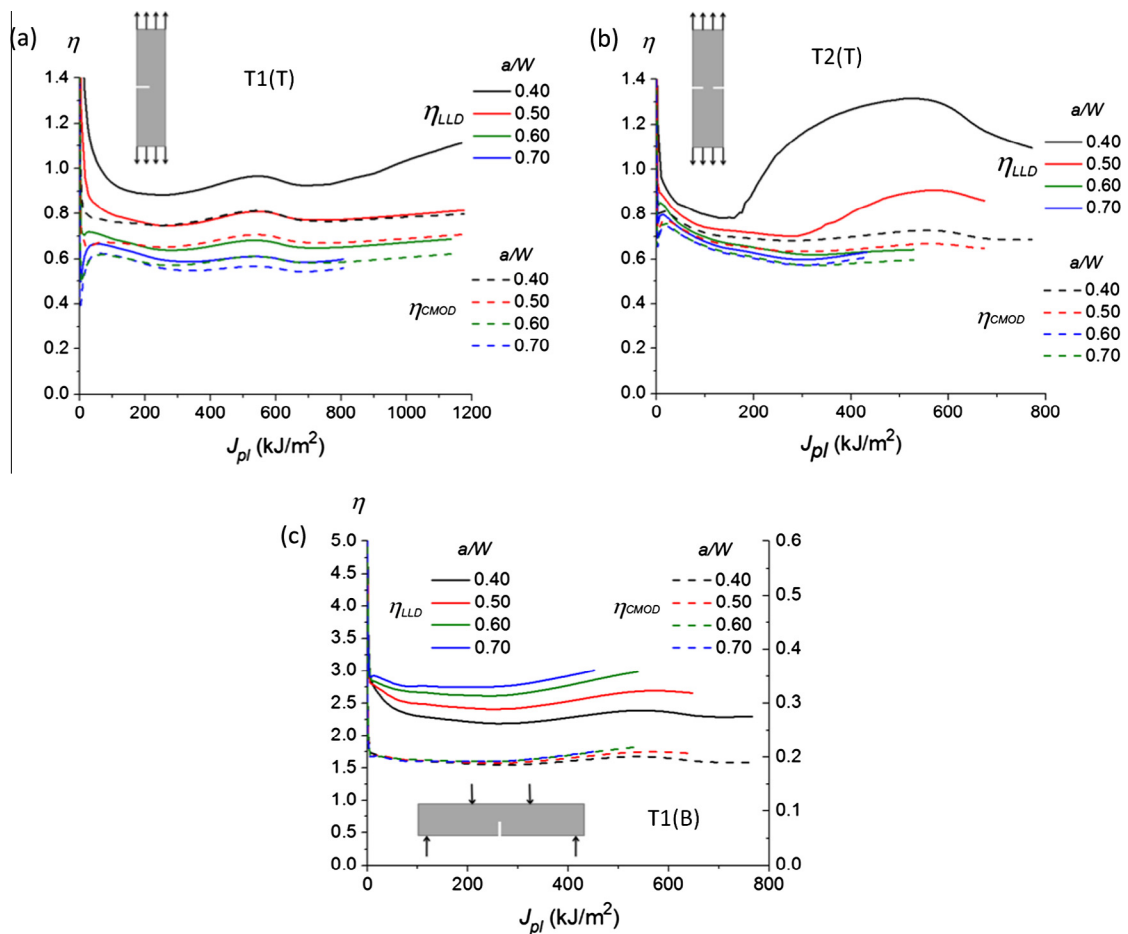
Fig. 5. Results of the η-factors vs. J_{pl} for specimens with circumferential TWCs: (a) T1(T), (b) T2(T) and (c) T1(B) specimens.

4.2. The η-factor results

This section presents the numerical results of the η-factor defined in terms of the *LLD* and the *CMOD*. Figs. 5 and 6 provide the η-factors for the proposed fracture test configurations with different a/W ratios. The η-factors were plotted in terms of the *J*-integral values in order to analyze the validity of the η-factor method. If the plots are horizontal lines, then the η-factor is independent of the loading level and the η-factor method can be considered acceptable. On the other hand, if the η-factor shows a dependency with the *J*-integral, then the η-factor method is not suitable for estimating the *J*-integral.

Fig. 5 shows the results for the specimens with circumferential TWCs, where solid lines represent the η_{LLD} and the dashed lines correspond to the η_{CMOD}.

In Fig. 6 are presented the results for specimens with longitudinal TWCs.

5. Discussion of results

The plots in Figs. 5 and 6 show that some degree of dependence exists between the η-factors values and the applied *J*-integral or, equivalently, the level of load or deformation. Assuming that less deformation level dependence of the η-factor implies more validity of the η-factor existence, some conclusions can be obtained from the previous results.

It can be seen that the extent of dependence is affected differently for low or high loads. In general, the effect at low or medium loads is more important for specimens with low constraint conditions, i.e., for shallow cracks or tensile loadings configurations. As the cracks become deeper, the η-factors tend to almost constant values for all specimens under research. Furthermore, the specimens under bending loads present η-factors with less dependence than the tensile specimens, even for the same ratios a/W. Therefore, bending configurations favor the validity of the η-factor method, unlike tensile loading configurations.

On the other hand, the η-factor based on *CMOD* showed low load or deformation level dependence, both in tensile and bending configurations. Using different material and specimen types, other authors [12–14,23] showed that the η-factors
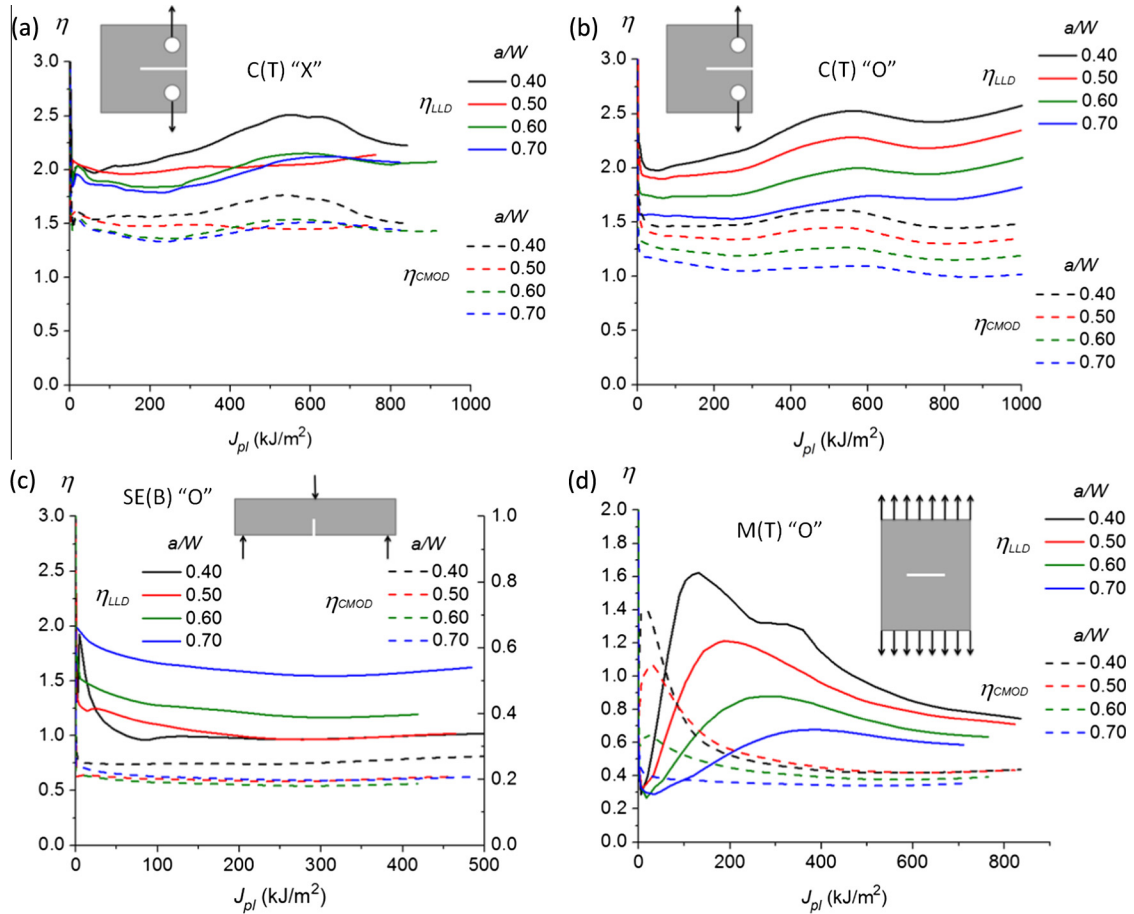
Fig. 6. Results of the η-factors vs. J_{pl} for specimens with longitudinal TWCs: (a) C(T) "X", (b) C(T) "O", (c) SE(B) "O" and (d) M(T) "O" specimens.

derived for *CMOD* are less sensitive to the loading or deformation levels and the material properties (i.e. strain hardening and yield stress) than the η-factors derived for *LLD*, specially for shallow cracks. This can be understood considering that the *CMOD* is a local measurement in the crack process region; then the area under the *P* vs. *CMOD* curve represents mainly the part of the plastic energy (or plastic work) associated with the crack growth process, excluding that part of the potential energy used in the plastic deformation of the specimen.

Cravero and Ruggieri [12] found in their numerical work a similar behavior for single-edge-notched tension specimens. They assumed that for low deformation levels, the elastic and plastic areas under the *P* vs. *LLD* or *P* vs. *CMOD* have similar magnitudes, thereby affecting the calculated η-factors. For higher loading levels or *J*-integral values, a region with a plateau is generally reached. For that region, Cravero and Ruggieri [12] considered reasonable to use an averaging procedure to compute the η-factors, arguing that the typical values of experimentally measured *J*-integrals in fracture testing are reached for the higher deformation levels. Following the same criterion, η-factors were estimated from the results in Figs. 5 and 6 considering the last part of the curves, taking an averaged value for each crack length. All the averages were calculated using the η-factors values for *J*-integrals higher than 100 kJ/m^2, excepting the case of the M(T) "O" specimens where the η-factors values used correspond to *J*-integrals higher than 500 and 300 kJ/m^2 for η_{LLD} and η_{CMOD}-factors, respectively. Fig. 7 resumes the averaged η-factors (η_{LLD} and η_{CMOD}) and their dependence with the crack length for all the specimens studied. Error bars are included indicating the maximum and minimum values of η-factors in the averaging region considered.

Regarding the validity of the η-factor method, it should be mentioned that the η-factors values reported in different standards for standardized specimens are not without some uncertainty. These expressions are usually derived from limit load analyses, i.e., assuming that the separability condition expressed in Eq. (3) is valid, while a perfectly plastic, non-hardening material behavior is adopted. According to Wallin [24], the uncertainty in standardized η-factors values is around 10%. Therefore, the η-factors obtained using the averaging process may result in acceptable values as long as its variation with the applied load is reduced. This is particularly true considering that the actual stress vs. strain tensile curve was used in the finite element analyses.
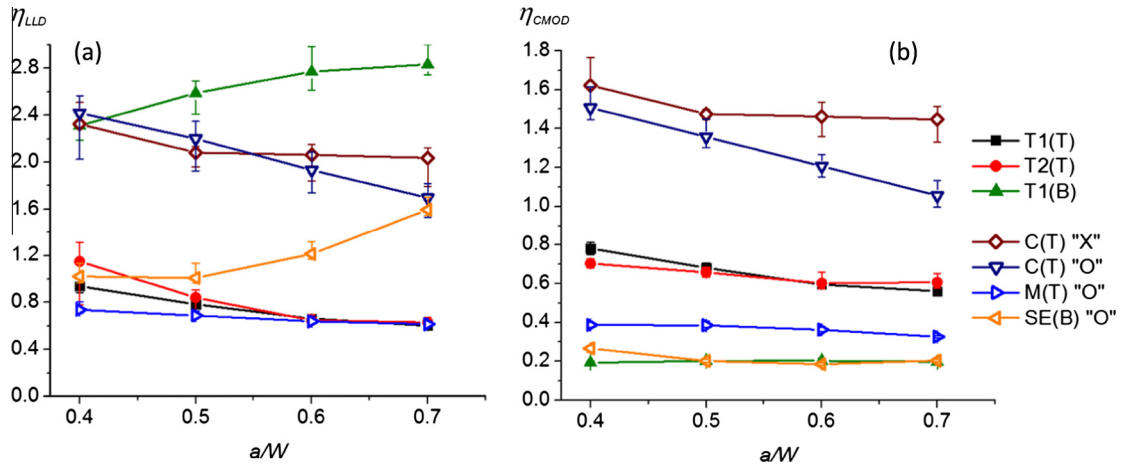
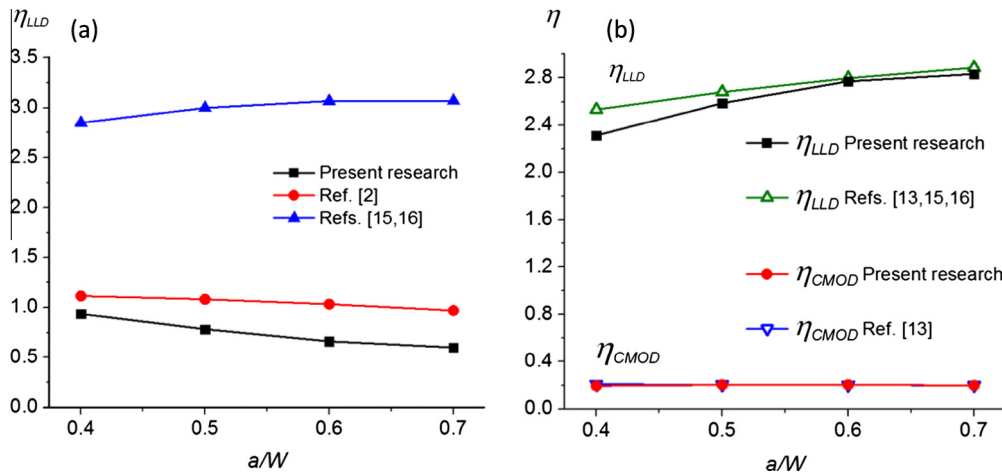**Fig. 7.** Results of the averaged η-factors vs. a/W for the specimens proposed: (a) η_{LLD}-factors and (b) η_{CMOD}-factors.

Fig. 8. Reported η-factors vs. a/W for specimens with circumferential TWCs: (a) η_{LLD}-factors for T1(T) specimens, (b) η_{LLD} and η_{CMOD}-factors for T1(B) specimens.

There are some expressions available in the literature for the η-factors for tubes with circumferential TWCs subjected to axial tension (only for T1(T) specimens) [2,15,16], and for bending tension (T1(B) specimens) [13,15,16].

For axial tension T1(T) specimens, some classical Refs. [15,16] propose an analytical derived expression for the η_{LLD}-factors. On the other hand, Huh et al. [2] present a fit of numerical results for the η_{LLD}-factors obtained from finite element simulations of specimens made of SGTs. Fig. 8(a) shows the above expressions with the values obtained in the present research. The comparison among these proposals shows an important disparity in the values, which was the motivation for a deeper study to verify the correctness of the definitions of η-factors for the particular geometries under research. It is believed that the discrepancy is due to different restraint conditions of the specimen ends. In the present research, as in [2,4], the specimen ends were considered as clamped, whilst in [15,16] the ends were free to rotate.

For the four point bending configuration T1(B), there are analytically derived expressions for the η_{LLD}-factors derived from limit load solutions (or, equivalently, from the $h(a/W)$ function in Eq. (3)) [15,16]. Gupta et al. [13] simulated four point bending tests for large pipes used in the primary heat transport of nuclear power plants, made of different low alloy carbon steels. They found a good agreement between the analytical and numerical η_{LLD}-factors. In addition, these authors proposed an analytical η_{CMOD}-factor that can be derived from the η_{LLD}-factor and geometric factors of the cracked tube, whose validity was confirmed from their numerical finite element results. In Fig. 8(b) the η_{LLD} and η_{CMOD}-factors obtained in this research are plotted with the results of Gupta et al. [13]. It can be seen a general good agreement between the values, with a maximum difference of 9%.

In the case of the specimens with longitudinal cracks, there are no similar references in open literature allowing for a numerical comparison. However, some general remarks can be obtained from Figs. 6 and 7.

For the C(T) type specimens, it is noticeable that the values of the η_{LLD}-factors are close to 2, which is approximately the value proposed in standards such as ASTM 1820 for plane C(T) specimens. This is an interesting result taking in mind that the stiffness of the C(T) "X" or C(T) "O" specimens is considerably lower than a plane C(T) specimen with an equivalent thickness. In other words, the numerical curves P vs. LLD or P vs. CMOD and J vs. P differ considerably among the three specimens, but the η_{LLD}-factors derived using Eq. (7) coincide reasonably to the same value.

In the case of the SE(B) "O" specimen, the η_{LLD}-factors reach values close to 2 for very deep cracks ($a/W > 0.7$), which in turn is the value for a pure bending configuration. However, for less deep cracks, the η_{LLD}-factors tend to lower values.

Finally, the η_{LLD}-factors for the M(T) "O" specimen range around 0.65, being 0.5 the typical value for plane specimens [25]. As in the previous case with the C(T) specimens, a great difference exists between the P vs. LLD or P vs. CMOD and J vs. P curves obtained for curved and plane M(T) "O" specimens, but the η_{LLD}-factors tend to a relatively similar value.

It should be noted that in all the non-standard specimens with longitudinal cracks, a bending component appears due to the geometry of the undeformed circumference arc of the original tube, tending to straighten the curvature of this region. Obviously, this bending component is not present in the case of plane specimens. Despite of this, the averaged η-factors estimated numerically here for curved specimens coincide reasonably with the values of standard plane specimens.

6. Conclusions

From the numerical research presented previously the following conclusions were obtained:

- The η-factor method validity depended, in some extent, on the testing configuration considered.
- Bending loadings favored the independence of the η-factor values regarding the load or deformation levels, so validating the η-factor method. On the other hand, tensile loadings promoted a higher degree of dependence of the η-factor with the load, reducing the certainty of J-integral values estimated through the η-factor method.
- In all cases, specimens with deep cracks showed less dependence of the η-factor with loading.
- The η-factor based on the CMOD was much less sensitive to the loading or deformation levels than the η-factor derived for LLD.
- A general good agreement was found between the averaged η-factors obtained in this work and the values of "similar-type" more standard plane specimens.

Summarizing, high constraint conditions favored the validity of the η-factor method for estimating the J-integral values with the non-standard specimens presented above.

It was also shown the usefulness of the numerical techniques to study the applicability of non-standard specimens for fracture testing, in terms of validity of the η-factor method and for the estimation of η-factor values for particular specimen geometries.

Acknowledgements

References

[1] Bergant M, Yawny A, Perez Ipiña J. Failure assessment diagram in structural integrity analysis of steam generator tubes. Proc Mater Sci 2015;8:128–38. http://dx.doi.org/10.1016/j.mspro.2015.04.056.
[2] Huh N, Kim J, Chang Y, Kim Y, Hwang S, Kim J. Elastic–plastic fracture mechanics assessment for steam generator tubes with through-wall cracks. Fatigue Fract Engng Mater Struct 2006;30:131–42. http://dx.doi.org/10.1111/j.1460-2695.2006.01094.x.
[3] Majumdar S. Failure and leakage through circumferential cracks in steam generator tubing during accident conditions. Int J Press Vessels Pip 1999;76:839–47. http://dx.doi.org/10.1016/S0308-0161(99)00058-7.
[4] Bergant M, Yawny A, Perez Ipiña J. Estimation procedure of J-resistance curves for through wall cracked steam generator tubes. Proc Mater Sci 2012;1:273–80. http://dx.doi.org/10.1016/j.mspro.2012.06.037.
[5] Sanyal G, Samal M. Investigation of fracture behavior of steam generator tubes of Indian PHWR using PLT specimens. Proc Engng 2013;55:578–84. http://dx.doi.org/10.1016/j.proeng.2013.03.298.
[6] Paris P, Ernst H, Turner C. A J-integral approach to development of η-factors. In: Fracture Mechanics: Twelfth Conference, ASTM STP 700, American Society for Testing and Materials; 1980. p. 338–50. http://dx.doi.org/10.1520/STP36979S.
[7] EPRI. Steam generator integrity assessment guidelines. Revision 2, Technical Report 1012987; 2006. p. 3.8.
[8] Rice J, Paris P, Merkle J. Some further results of J-integral analysis and estimates. In: Progress in flaw growth and fracture toughness testing, ASTM STP 536, Philadelphia, American Society for Testing and Materials; 1973. p. 231–45. http://dx.doi.org/10.1520/STP49643S.
[9] Sumpter J, Turner C. Method for laboratory determination on Jc. In: Cracks and fracture, ASTM STP 601. American Society for Testing and Materials; 1976. p. 3–18. http://dx.doi.org/10.1520/STP28634S.
[10] Ernst H, Paris P, Landes J. Estimations on J-integral and tearing modulus t from a single specimen test record. In: Roberts R, editor. Fracture mechanics: thirteenth conference, ASTM STP 743. American Society for Testing and Materials; 1981. p. 476–502. http://dx.doi.org/10.1520/STP28814S.
[11] Turner C. The ubiquitous η factor. In: Fracture mechanics: twelfth conference, ASTM STP 700. American Society for Testing and Materials; 1980. p. 314–37. http://dx.doi.org/10.1520/STP36978S.
[12] Cravero S, Ruggieri C. Estimation procedure of J-resistance curves for SE(T) fracture specimens using unloading compliance. Engng Fract Mech 2007;74:2735–57. http://dx.doi.org/10.1016/j.engfracmech.2007.01.012.

[13] Gupta S, Bhasin V, Vaze K, Ghosh A, Kushwaha H, Chapuliot S, et al. Derivation of J-resistance curve for through wall cracked pipes from crack mouth opening displacement. Int J Press Vessels Pip 2006;83:686–99. http://dx.doi.org/10.1016/j.ijpvp.2006.05.004.

[14] Suh N, Kim Y. Determination of J-integral using the Load-COD record for circumferential through-wall cracked pipes. J Pressure Vessel Technol 2008;130:1–4. http://dx.doi.org/10.1115/1.2967830.

[15] Zahoor A. Ductile fracture handbook, EPRI-NP-6301-D, N14-1, Research Project 1757-69, Electric Power Research Institute; 1989–1991.

[16] Chattopadhyay J, Dutta BK, Kushwaha HS. Derivation of 'γ' parameter from limit load expression of cracked component to evaluate J-R curve. Int J Press Vessels Pip 2001;78:401–27. http://dx.doi.org/10.1016/S0308-0161(01)00053-9.

[17] Cravero S, Ruggieri C. Further developments in J evaluation for growing cracks based on LLD and CMOD data. Int J Fract 2007;148:387–400. http://dx.doi.org/10.1007/s10704-008-9211-9.

[18] Schwalbe KH, Newman Jr JC, Shannon Jr JL. Fracture mechanics testing on specimens with low constraint-standardisation activities within ISO and ASTM. Engng Fract Mech 2005;72:557–76. http://dx.doi.org/10.1016/j.engfracmech.2004.04.006.

[19] Schwalbe KH, Heerens J. R-curve testing and its relevance to structural assessment. Fatigue Fract Engng Mater Struct 1998;21:1259–71. http://dx.doi.org/10.1046/j.1460-2695.1998.00110.x.

[20] Newman Jr JC, Crews Jr JH, Bigelow CA, Dawicke DS. Variations of a global constraint factor in cracked bodies under tension and bending loads. In: Kirk M, Bakker A, editors. Constraint effects in fracture theory and applications: second volume, ASTM STP 1244; 1995. p. 21–41. http://dx.doi.org/10.1520/STP14629S.

[21] Brocks W, Scheider I. Numerical aspects of the path-dependence of the J-integral in incremental plasticity, Technical Note GKSS/WMS/01/08, Institut für Werkstofforschung, GKSS-Forschungszentrum Geesthacht; 2001. p. 13.

[22] ABAQUS/Standard Version 6.12-1, User's Manual, 11.4.2 Contour integral evaluation; 2012.

[23] Zhu X, Leis B, Joyce J. Experimental estimation of J–R Curves from Load-CMOD record for SE(B) specimens. J ASTM Int 2008;5:66–86. http://dx.doi.org/10.1520/JAI101532.

[24] Wallin K. Fracture toughness of engineering materials, estimation and application. Warrington, UK: EMAS Publishing; 2011. p. 20.

[25] Wu S, Mai Y, Cotterell B. Plastic η-factor (ηp) of fracture specimens with deep and shallow cracks. Int J Fract 1990;45:1–18. http://dx.doi.org/10.1007/BF00012606.